Improved design of large wind turbine blade of fibre composites based on studies of scale effects (Phase 1). Summary report

Sørensen, Bent F.; Jørgensen, E.; Debel, C.P.; Jensen, Find Mølholt; Jensen, H.M.; Jacobsen, T.K.; Halling, K.

Publication date:
2004

Document Version
Publisher's PDF, also known as Version of record

Risø-R-1390(EN)

Improved design of large wind turbine blade of fibre composites based on studies of scale effects (Phase 1) - Summary Report

Bent F. Sørensen[#], Erik Jørgensen*, Christian P. Debel[#]*, Find M. Jensen*, Henrik M. Jensen[$], Torben K. Jacobsen[¤] and Kaj M. Halling[+]

[#]Materials Research Department, Risø National Laboratory, 4000 Roskilde, Denmark
*Wind Energy Department, Risø National Laboratory, 4000 Roskilde, Denmark
[$]Department of Solid Mechanics, The Technical University of Denmark, 2800 Lyngby, Denmark, Present adress: Department of Building Technology and Structural Engineering, Aalborg University, 9000 Aalborg, Denmark
[¤] LM Glasfiber A/S, Rolls Møllevej 1, 6640 Lunderskov, Denmark
[+]Vestas Wind Systems A/S, E. F. Jacobsens Vej 7, 6950 Ringkøbing, Denmark

Risø National Laboratory
Roskilde
Denmark
September 2004

Author: Bent F. Sørensen, Erik Jørgensen, Christian P. Debel, Find M. Jensen, Henrik M. Jensen, Torben K. Jacobsen and Kaj M.Halling
Title: Improved design of large wind turbine blade of fibre composites based on studies of scale effects (Phase 1) - Summary Report

Department: Materials Research Department

Risø-R-1390(EN)
September 2004

Abstract

The main aim of the present study was to enhance the understanding of damage evolution in wind turbine blades by a combination of structural- and material modelling. Basic damage modes were identified in wind turbines tested to failure under static and cyclic loadings. Two of the observed damage types, compression failure and crack growth along adhesive joints, were studied in details. Modelling of a load carrying composite spars as well as composite columns were performed for assessing the compressive strength. A fracture mechanics approach was developed for prediction the strength of adhesive joints. The effect of porosity on the strength of adhesive joints was also investigated.

ISSN 0106-2840
ISBN 87-550-3176-5
87-550-3177-3 (Internet)

Contract no.:
1363/01-01-0007

Group's own reg. no.:
1615052-00

Sponsorship:
EFP 2001

Cover :

Pages: 36
Figures: 39
References: 28

Risø National Laboratory
Information Service Department
P.O.Box 49
DK-4000 Roskilde
Denmark
Telephone +45 46 77 40 04
bibl@risoe.dk
Fax +45 46774013
www.risoe.dk

Contents

Preface

This summary-report contains a sort summary of the activities of a project called "Improved design for large wind turbine blades, based on studies of scale-effects (Phase 1)", partially supported by the Danish Energy Authority under the Ministry of Economics and Business Affairs through a EFP2001-fund (journal no. 1363/01-01-0007). The project ran 1½ year from 2001 to 2002. The participants in the project were: The Materials Research Department, Risø National Laboratory (project leader), The Wind Energy Department, Risø National Laboratory, The Department of Mechanical Engineering (Solid Mechanics), The Technical University of Denmark, Department of Mechanical Engineering, Aalborg University, LM Glasfiber A/S and Vestas Wind Systems A/S. It was found to be impossible to acquire students at Aalborg University. As a result, no work was performed there. Instead, more work was carried out at Risø National Laboratory.

This summary-report only contains the major results of the project. A throughout description of the work can be found in the publications listed towards the end of this report.

1 Introduction

1.1 Background

There is strong drive in the wind turbine industry for the development of yet larger and larger wind turbines. This rapid up scaling creates a need for better design tool, since it becomes essential to save material not only to reduce cost (volume of material used), but also to reduce the gravitational forces. This is particularly true for wind turbine blades, which are the largest rotating component of a wind turbine.

Wind turbine blades are usually made in polymer matrix composites, often glued together. Such structures may develop a number of failure modes. However, the understanding of failure in fibre composites is not nearly as advanced as for failure of metals. Throughout more than a century, knowledge has been established on how different processing conditions (alloy composition, heat treatments etc.) control microstructures and strength properties of metals. It is thus possible to specify how processing conditions should be to make metals that have the desired mechanical properties. Moreover, it is possible by microstructural investigations (e.g. optical microscopy) to assess the strength properties of metals. In contrast, such a comprehensive understanding does not yet exist for fibre composites, partly because there are many mode failure modes in composites and partly because fibre composites constitute a relative new material class. Obviously, there is a need for much more knowledge in this area.

Relative large partial coefficients are used for the strength properties of composite materials used in wind turbine blades (Christensen et al., 2000). That is largely to account for material variation and for uncertainties related to the models for strength and lifetime predictions; the present design approach does no contain criteria for many of the possible failure modes. To compensate for this, modern wind turbine blades must undergo a detailed full-scale test to be certified. However, in the recent years more unexpected failures have occurred during these certification tests in the recent years, indicating that the present design tools are insufficient.

1.2 Purpose

This project represents a step towards the creation of a coherent understanding of failure in composite structures from microscale (fibre/matrix level) to component level. The long-term goal is to develop *general approaches* and *generic models* for each possible failure modes, so that the material properties can be fully utilised and the structural design can be optimised. This will result in new design methods for the industry. The specific purpose of this project (Phase 1) was to study scale effects, in particular to classify the failure modes in wind turbine blades (from blades tested to failure), to enhance the understanding of failure in composite structures under compressive loading and develop approaches for experimental characterisation and modelling of adhesive joints under mixed mode (from pure peel to pure shear) loading.

This report is a summary report of the project, and contains only a brief presentation of the major results. More details can be found in the technical reports or publications made throughout the project. These publications are listed in the end of this report.

2 Full scale test of wind turbine blade to failure

A 25 m wind turbine blade (type V52, provided by Vestas Wind Systems A/S), was tested to failure by loads in the flapwise direction (Jørgensen et al., 2004). Prior to these test, the blade had undergone a full-scale extreme load and cyclic loading corresponding to a 20-year fatigue life. The purpose of the test was to gain detailed information about failure mechanisms in a wind turbine blade especially with focus on failures in the compression side of the blade. Prior to the tests the blade was inspected by ultrasonic scanning to get an overview if any imperfections and damages were present already before starting the test. The supports and loading of the blade was such that it was possible to use the same blade in three tests, i.e. having independent failures in three different sections of the blade. During each of the tests the behaviour of the blade was recorded by means of video and photos, strain gauges, acoustic emission and deflection sensors. Two different types of deflection sensors were mounted on the blade, one giving the total deflection of the blade and another giving skin and main spare displacements, locally. Each test was stopped at every sign of damage and inspected visually and cracks and propagation of damages were identified.

2.1 Test setup and sensoring systems

Three different loads cases were applied to the blade in order to generate three independent failures in a single blade. The sections to test were decided based on knowledge of the compression strength and the blade geometry. The next task was then to find out how to load and support the blade so that the failures did not happen in regions close to the yokes for support and load inputs. The design strength of the blade was known from the manufacturer and the task was then to achieve a distribution of the bending moment (*M*) in the blade to have the damage in a desired region. The three different test setups, showing where the loads and supports were put to get the failures at the predetermined locations, are shown in Figs. 2.1 to 2.3. In test no. 2, a more complex loading setup with two forces of uneven magnitude, in opposite directions, was required to initiate failure, at least according to the strength calculations, at the chosen location.

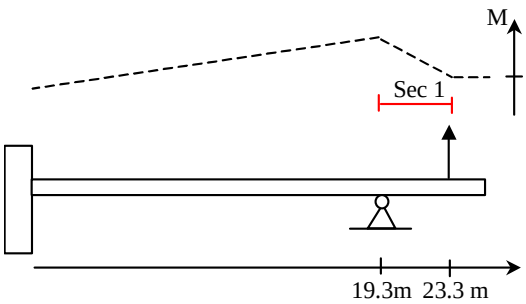

Fig. 2.1 Supports and load inputs in the test of section 1. The magnitude of the applied moment, M*, is shown by a dashed line.*

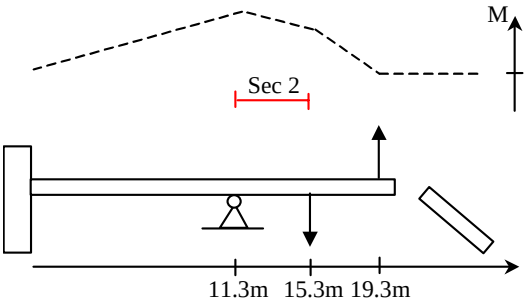

Fig. 2.2 Supports and load inputs in the test of section 2. By the use of two forces it is possible to vary the moment distribution along the test section.

Before applying the loads, the areas of the three test sections were inspected by ultrasound scanning in order to locate any damages or imperfections that might be present in the blade before starting the test. A simple tap test was also done with the same purpose. These imperfect areas, primary areas with lack of glue or delaminations, were marked and the propagation was followed during the tests. This also made it possible to state whether these imperfections actually were causing the final failure of the blade.

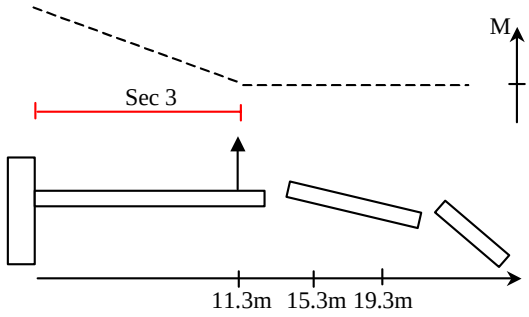

Fig. 2.3 Supports and load inputs in the test of section 3.

During the tests the structural behavior of the blade was monitored with many sensors. The load was measured with a load sensor at the point of load application. The global deflection was also measured at the location of the load application. Local skin deflections were measured in the test section at five locations by the use of LVDTs mounted in special holders, see Fig. 2.4. Strain measurements were done along the blade and also inside the main spare. More than a hundred strain gauges were mounted on the blade to give the axial strain and at a few locations rosette gauges were mounted. In case of no linearity between deflection/strain and the load the test was stopped and the blade inspected for any damages.

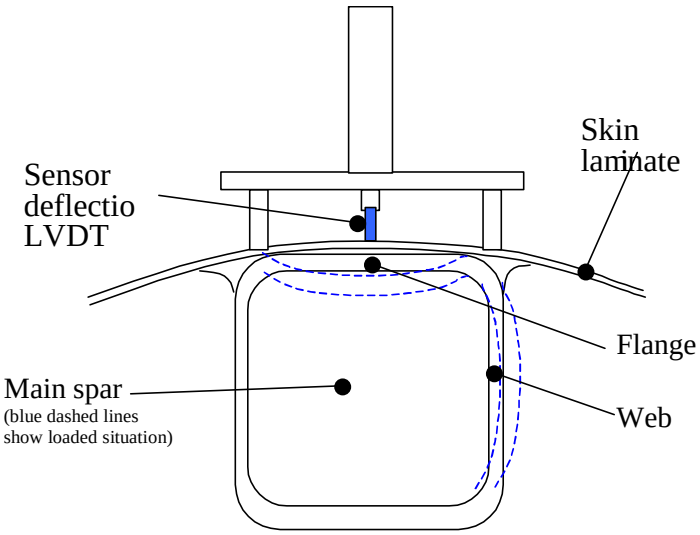

Fig. 2.4 Sketch of the system for measuring local deflections on top of the main spar.

Acoustic emission of the blade was measured during the test to identify failures and locations of the damages in the blade. Two separate systems were used: A SPARTAN AT system records the waveform characteristics of the AE signals (amplitude, rise time, energy, etc.) on two channels and a Labview system is based around a high-speed data card which can digitize and record the entire waveform of the AE signals on four channels. Both systems are sensitive enough to detect signals resulting from very small damage at the very early stages of the test.

2.2 Test results

The global deflection of the blade was found not to be very sensitive to the damage that happens in the blade. It is therefore very difficult to give any criteria based on the global deflection about how close the blade is to failure. Fig. 2.5 shows the deflection of the blade (Test section 1) before failure and Fig. 2.6 shows the failure zone in the blade just after fracture.

Fig. 2.5 Test of section 1; the blade deflects sigificantly before failure occurs.

Fig. 2.6 Failure of section 1

The local deflection is shown versus the load in Fig. 2.7 and the graph shows clearly, how the deflection grows without applying more loads, i.e. the curve becomes flat when the load is close to the load of failure of the section (last point in this curve).

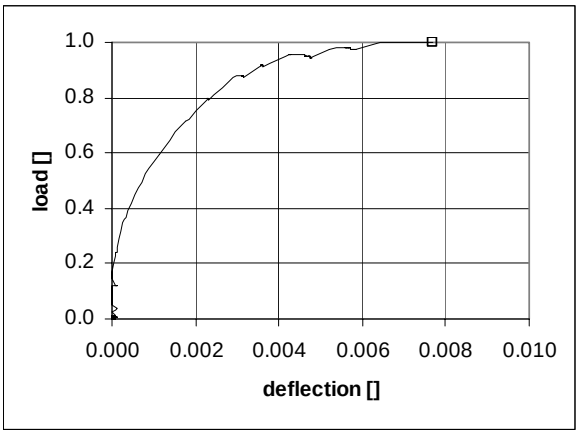

Fig. 2.7 Local deflection at 4.3 m, load at 11.3 m.

During the tests, acoustic emission from the blade was also measured. It was proved to be a very promising method to use during static tests of blades. The measurement gave information concerning the severe ness as well as the localization of the damages in the blade. Fig. 2.8 shows how the acoustic activity increases when getting close to the failure and also how this activity continues for a long time although the load is kept constant (or decreases slightly).

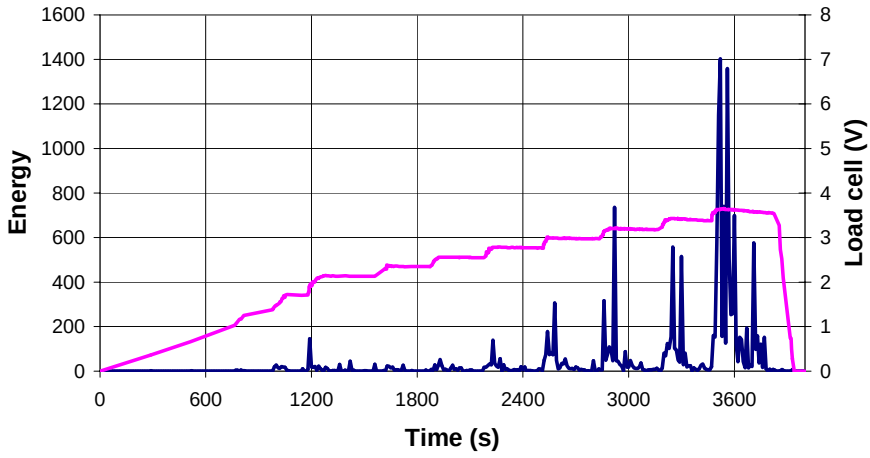

Fig. 2.8 Stress wave activity (dark blue) detected during step-wise loading of the blade (section 2), shown along with the load level (pink) as a function of elapsed test time. The high activity levels and long "die-off" time during load hold (nearly constant load) indicate that the blade is close to failure.

AE was also found to be very useful as a tool assisting the test procedure. As an example, during test of section number 3, a significant amount of AE activity was detected at a yoke attached to the load carrying spar. This suggested, that the main spar was beginning o fail at the yoke. Therefore, in order to avoid further damage development there, a wood block was made and inserted into the spar, giving internal support. As a result, no further damage development took place at the yoke. Instead, a valid failure was obtained for Test Section 3.

2.3 Summary and conclusion

The test of the 25 m Vestas blade showed good results using ultrasonics to scan the blade for irregularities especially in the interface between the relative thin skin laminate and the load carrying main spar. The detection of areas where glue was missing was easy to identify on the basis of the images form the scans.

The method of measuring local deflections of the main spar and skin laminate with the equipment developed in the project seems to be very promising and can be useful for determination of how close the blade is to a failure and for calibration of FE models of blades. Strain gauge measurements also give good indication of

how close the blade is to a failure, i.e. by showing non-linear behavior. The total deflection of the blade does not show clearly a non-linear behavior when the blade is close to a failure.

For large deflections during a static test, it is preferable also to measure the angle by which the load is applied to give the possibility of calculating the real local bending moment. The practical benefits of the AE monitoring were seen in the three tests. These include identification of unwanted damages at load yokes, identification of damages making it possible to stop test and investigate damage and finally identification of how close you are to failure. The tests has given a large number of strain gauge measurement, local and global deflection measurements for three different sections of a wind turbine in flapwise load situations up to failure. The description of all the damages is fully described elsewhere (Jørgensen et al., 2003).

3 Post mortem analysis: observed failure modes

3.1 Abstract

It is of importance to identify the failure types that can develop in wind turbine blades, so that appropriate failure criterion can be developed and used in the design of future blades.

The present chapter of this summary report concerns the identification of different types of damage that developed in the three test sections of the Vestas A/S V52 wind turbine blade tested to failure under quasi-static loading, as briefly described in chapter 2. A post mortem investigation was carried out by cutting-up the failed test sections of the blade. Main emphasis is given to test section 1. Also, three wind turbine blades from LM Glasfiber A/S (type LM19.1), which, in another project (UVE, J.No. 51171/97-0043), were subjected to cyclic loading until failure was detected visually, were subjected to a post mortem analysis. Results for those blades will not be discussed here; however, details are given in Debel (2004).

3.2 Basic laminate-and-sandwich-scale-length damage types

Wind turbine blades are usually made of fibre composite structures, including sandwich structures, joined by adhesive layers. A number of failure mechanisms are possible at various length scales, ranking from failure of individual fibres to overall structural failure. A review of the most important damage types with regard to the laminate- and sandwich-scale is presented in the following.

Fig. 3.1 shows the main elements of a wing turbine blade and introduces a co-ordinate system, and Fig. 3.2 defines the different structural elements of a blade. The structure of the V52 blade from Vestas Wind Systems A/S was made up of a single box-shaped load carrying main spar, and of an aerodynamic shell consisting of an upwind and a downwind skin. The skins were glued to the main spar flanges by adhesive layers. Also, the skins were glued to each other along the leading edge and trailing edge joints by adhesive layers.

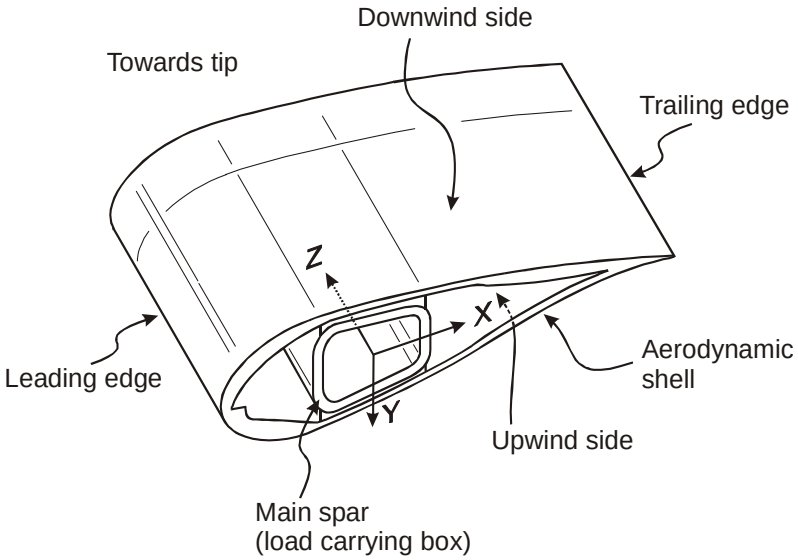

Fig. 3.1: The main elements of a wing turbine blade and definition of an XYZ coordinate system. (Fig._wind_turbine_elements.doc)

In the main spar, the load-carrying flanges towards the skins consisted of laminate, and the main spar walls (webs) towards the leading and trailing edges were a sandwich laminate/core/laminate structure. The skins in the X-direction towards the leading edge as well as towards the trailing edge consisted of a sandwich laminate/core/laminate structure (fibre orientation +/- 45^{o}).

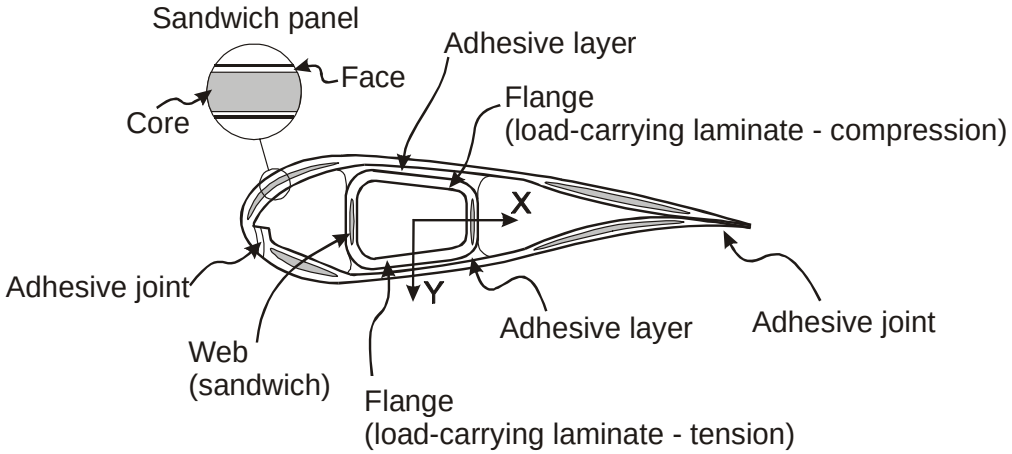

Fig. 3.2: Nomenclature of the different blade construction elements. (Fig._wind_turbine_elements.doc)

After the failure of each test section, the section was cut from the blade and examined. Emphasis was given to the structural members exposed to a compressive load, i.e. the main spar flange facing the downwind skin, as well as the downwind skin itself.

At first, all damages visible were documented using photos and sketches. Subsequently, the section was cut up further, and the damages found were examined and documented in details, again employing photos and sketches. The position of the damages and the types of damages were identified and divided into the basic types of damages listed below.

3.3 Types of damage observed: an overview

The processes involved in the failure of a specific blade may include several types of damage in the load-carrying structural members of the blade: the skins and the main spar (Debel, 2004). The types of damage found in the present study were categorised as follows:

Type 1: Damage formation and growth in the adhesive layer joining skin and main spar flanges *(skin/adhesive debonding* and/or *main spar/adhesive layer debonding)*;

Type 2: Damage formation and growth in the adhesive layer joining the up- and downwind skins along leading and/or trailing edges *(adhesive joint failure between skins)*;

Type 3: Damage formation and growth at the interface between face and core in sandwich panels in skins and main spar web *(sandwich panel face/core debonding)*;

Type 4: Internal damage formation and growth in laminates in skin and/or main spar flanges, under a tensile or compression load *(delamination driven by a tensional or a buckling load)*;

Type 5: Splitting and fracture of separate fibres in laminates of the skin and main spar *(fibre failure in tension; laminate failure in compression)*;

Type 6: Buckling of the skin due to damage formation and growth in the bond between skin and main spar under compressive load *(skin/adhesive debonding induced by buckling, a specific type 1 case)*;

Type 7: Formation and growth of cracks in the gel-coat; debonding of the gel-coat from the skin *(gel-coat cracking and gel-coat/skin debonding).*

3.4 Illustrations of observed damage types

Test section 1 failed at a distance from the root of about 20.1 meters; that is about in the middle of the test section. A sketch of some of the damage types found in this test section during the examination is given in Fig. 3.3. Fig. 3.4 shows the post failure damage, caused to the leading edge, at a stage where the blade still is supported by the unengaged loading chain. Following the disengagement of the loading chain, section 1 was cut from the blade and examined as described above.

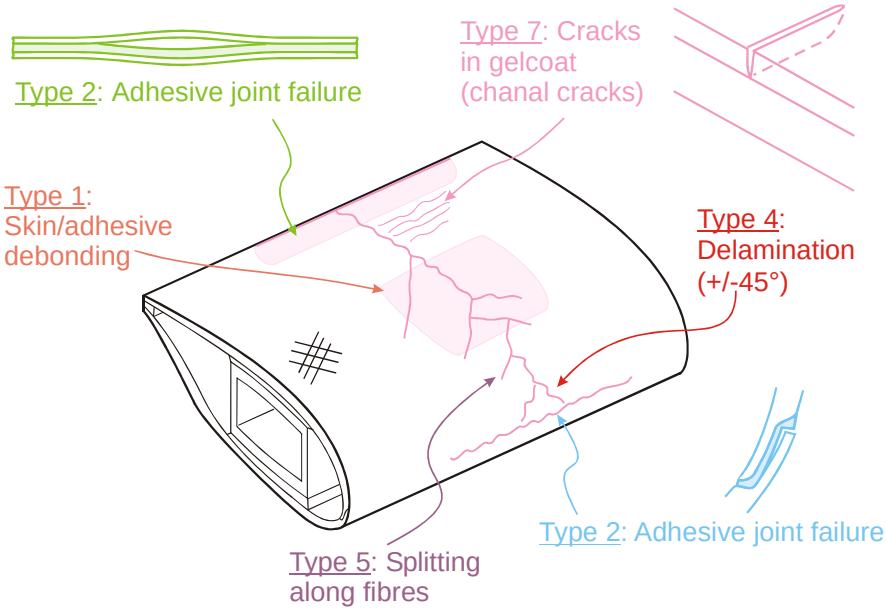

Fig. 3.3: Sketch illustrating of some of the damage types found during the examination of the downwind skin of test section 1 subjected to a compressive load. Damages to the adhesive layers: Types 1 (skin/adhesive debonding) *and 2* (adhesive joint failure between skins) *at the leading as well as the trailing edge. Damage to the downwind skin under compressive load: Types 4* (delamination driven by a buckling load), *5* (laminate failure in compression) *and 7* (gel-coat cracking and gel-coat/skin debonding). *(BSQR_Skitser_af_brudmåder_Vestasvinge_b.doc)*

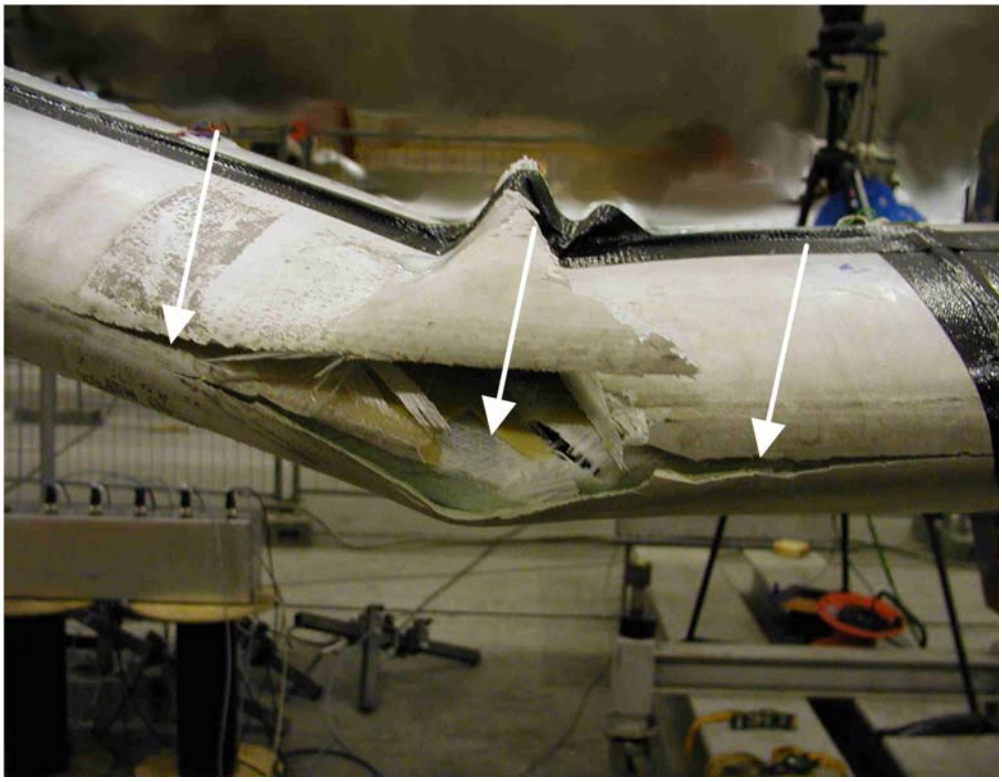

Fig. 3.4: The damage in test section 1 at the leading edge: Type 2 (adhesive joint failure between skins) at the arrows. The blade is still under load by the unengaged outer yoke. (D - P9250083m.jpg)

Fig. 3.5 illustrates compressive load damage caused to the downwind skin in at the leading edge. Damage types:

- Type 5 *(laminate failure in compression)* and
- Types 7 (gel-coat cracking and gel-coat/skin debonding) are identified.

The compression damage caused to the inside surface of the downwind skin of Fig. 3.5 is shown in Fig. 3.6. Again damage type:

- Type 5 *(laminate failure in compression)* is noticed, and furthermore damage type
- Type 3 *(sandwich panel face/core debonding)* is noticed in the downwind skin laminate.

Fig. 3.7 makes up a sketch of the damages found on the main spar outer surface facing the leading edge. These damages are further shown in the photos in Fig. 3.8:

- Type 3 *(sandwich panel face/core debonding)*
- Type 4 *(delamination driven by a tensional or a buckling load)*
- Type 5 *(fibre failure in tension; laminate failure in compression)*
- Type 6 *(skin/adhesive debonding induced by buckling, a specific type 1 case)*
- Type 7 *(gel-coat cracking and gel-coat/skin debonding).*

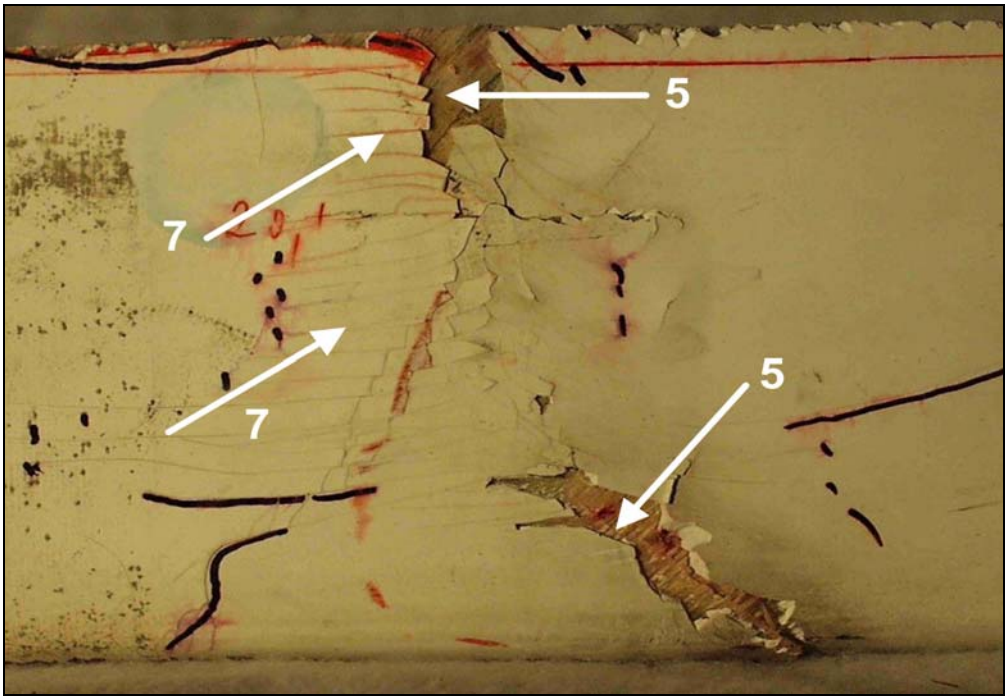

Fig. 3.5: Compressive load damage caused to the downwind skin at the leading edge (at the bottom). Damage Types 5 (laminate failure in compression/splitting) *and 7* (gel-coat cracking and gel-coat/skin debonding) *are identified. (D - sec1-damage-leading edge-compression.jpg)*

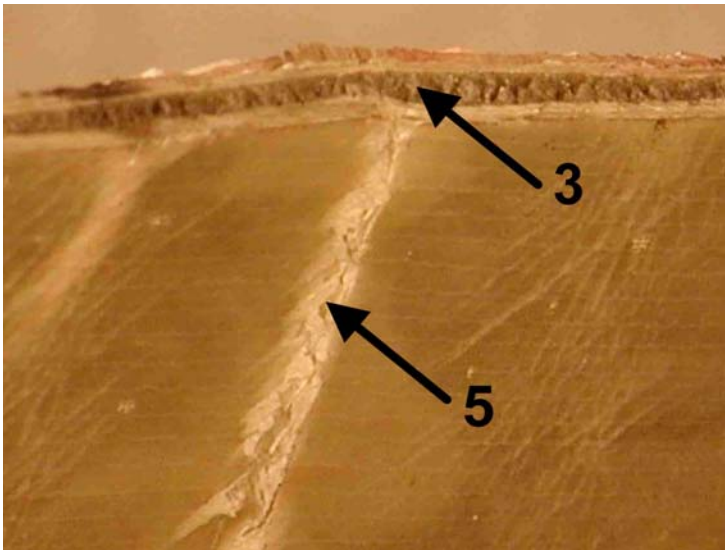

Fig. 3.6: Compression damage on the inside surface of the downwind skin shown in Fig. 3.6. Damage type 5 (splitting & compressive failure of skin laminate fibres). (D - sec1-damage-inside leading edge-2.jpg)

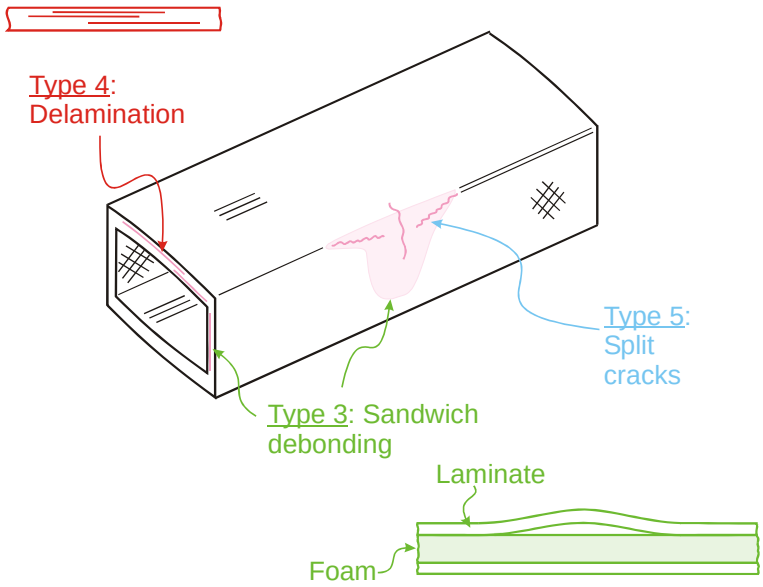

Fig. 3.7: Sketch showing visible damage to main spar outer surface: types 3 (sandwich panel face/core debonding), 4 (delamination driven by a buckling load) and 5 (fibre failure in tension; laminate failure in compression). (BSQR_Skitser_af_brudmåder_Vestasvinge-b.doc)

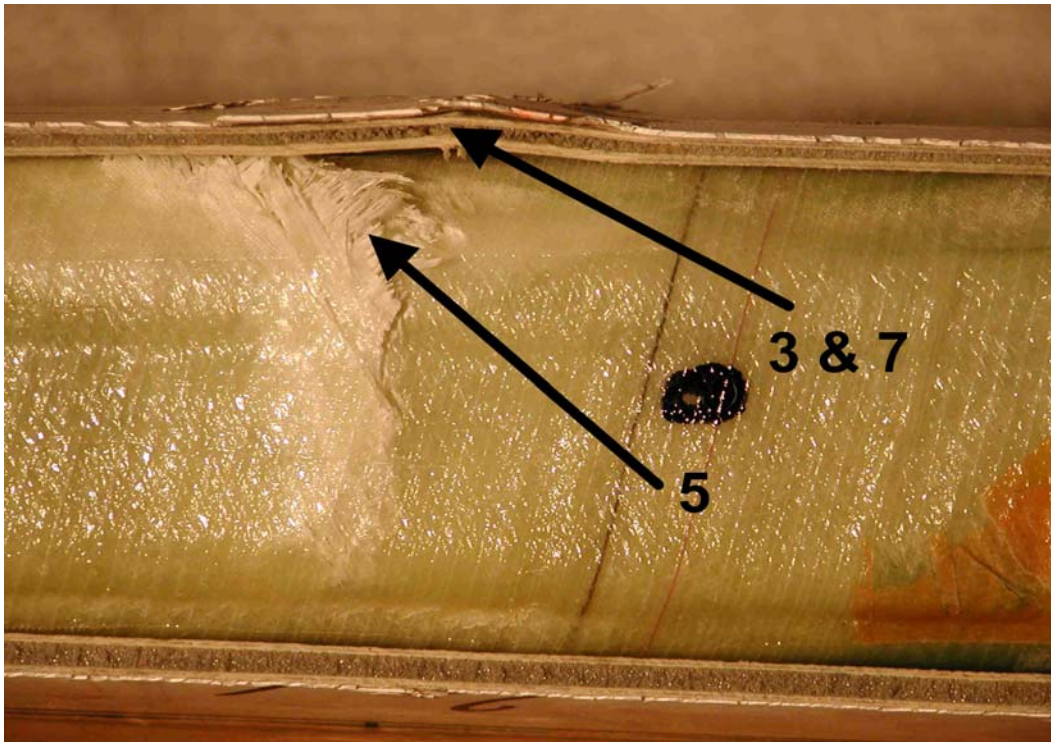

Fig. 3.8: Outer surface of the main spar facing towards the leading edge; cuts in the upper (top) and lower skins. Upper part of the structure was exposed to a compressive load. Damage types 3 (sandwich panel face/core debonding), 5 (laminate failure in compression) and 7 (gel-coat cracking and gel-coat/skin debonding). (D - outer surf, web vs lead-edge.jpg)

A sketch of the visible damage caused to the internal surface of the main spar after cutting-up is given in Fig. 3.9:

- Type 4 *(compression delamination)* in the upper flange laminate and
- Type 5 (*splitting & tensile failure of main spar fibres)* in the web.
- Type 1: skin/adhesive debonding has occurred.

Furthermore it is noticed, that the glue layer between the upper skin and the main spar upper flange is incompletely applied.

Finally, the sketch drawn up in Fig. 3.10 illustrates an additional damage – an internal, non-visible damage - inflicted onto the main spar:

- Type 4 *(a buckling-driven delamination of the main spar web)* damage.

The failure of test section 2 was quite similar to that of test section 1. However, unintended this section of the blade failed at the edge of the restraining yoke at position 15.3 metres from the root, not at its centre as was the case regarding test section 1. The post-mortem examination of test section 2 disclosed damage types rather similar to those found in test section 1.

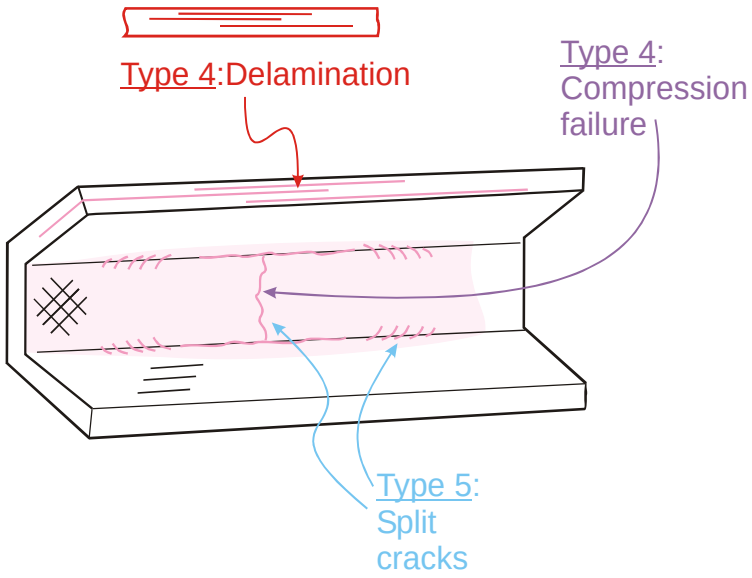

Fig. 3.9: Sketch of the visible damage caused to the internal surface facing the leading edge of the main spar after cutting-up. Upper part of the structure was exposed to a compressive load: Damage types 4 (delamination driven by buckling load) *in upper flange and 5 (*fibre failure in tension; laminate failure in compression) *in the web. (BSQR_Skitser_af_brudmåder_Vestasvinge-b.doc)*

Fig. 3.11 illustrates the downwind skin and the main spar flange of test section 2 and reveals damage types:

- Type 1 *(main spar flange/adhesive layer debonding)* and
- Type 4 *(delamination driven by a buckling load)* of the spar flange laminate.

The damage type 3 *(web sandwich panel face/core debonding)* is noticed in Fig. 3.13. Damage growth took place at the laminate/core interface, but a deviation of the damage path into the core material is also noticed.

Test section 3 failed at a distance from the root of about 4.4 metres by the bulging of the downwind skin in the middle of the section, causing all 7 failure types. The main spar web facing the leading edge is noticed in Fig. 3.12. Damage growth took place at the laminate/core interface, but a deviation of the damage path into the core material is also noticed.

3.5 Summary

Different types of damage that developed in the three test sections of a wind turbine blade tested to failure under quasi-static loading was identified, employing a post mortem investigation of damaged samples cut from the failed test sections of the main spar and the aerodynamic shell.

A total of seven different damage types were identified in the failed laminate and sandwich structures examined. The damage types involved damage formation and growth in laminates, adhesive joints, and sandwich panels.

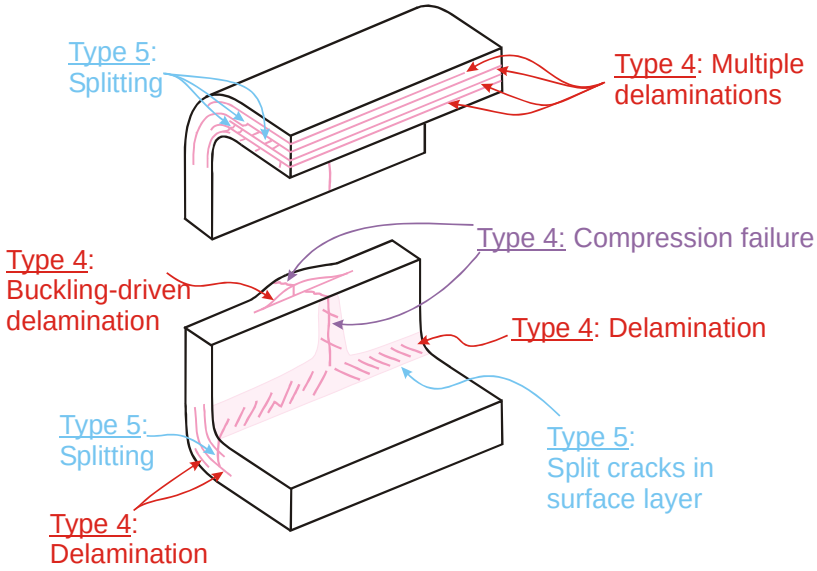

Fig. 3.10: Non-visible type 4 damage inflicted onto the main spar (delamination driven by a tensional or a buckling load) *as well as multiple type 5 damages* (fibre failure in tension; laminate failure in compression) *in the flanges. (BSQR_Skitser_af_brudmåder_Vestasvinge_b.doc)*

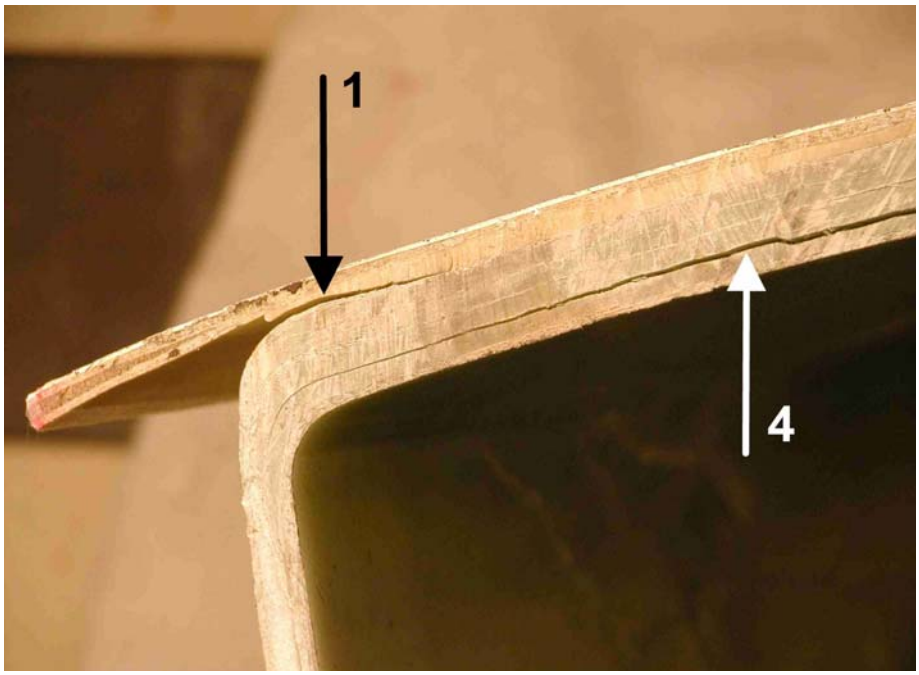

Fig. 3.11: Downwind skin and main spar flange of test section 2. Damage types 1 (main spar flange/adhesive layer debonding) *and 4* (delamination driven by a buckling load). *(D - skin-main spar adhersive layer debonding and main spar laminate debonding.jpg)*

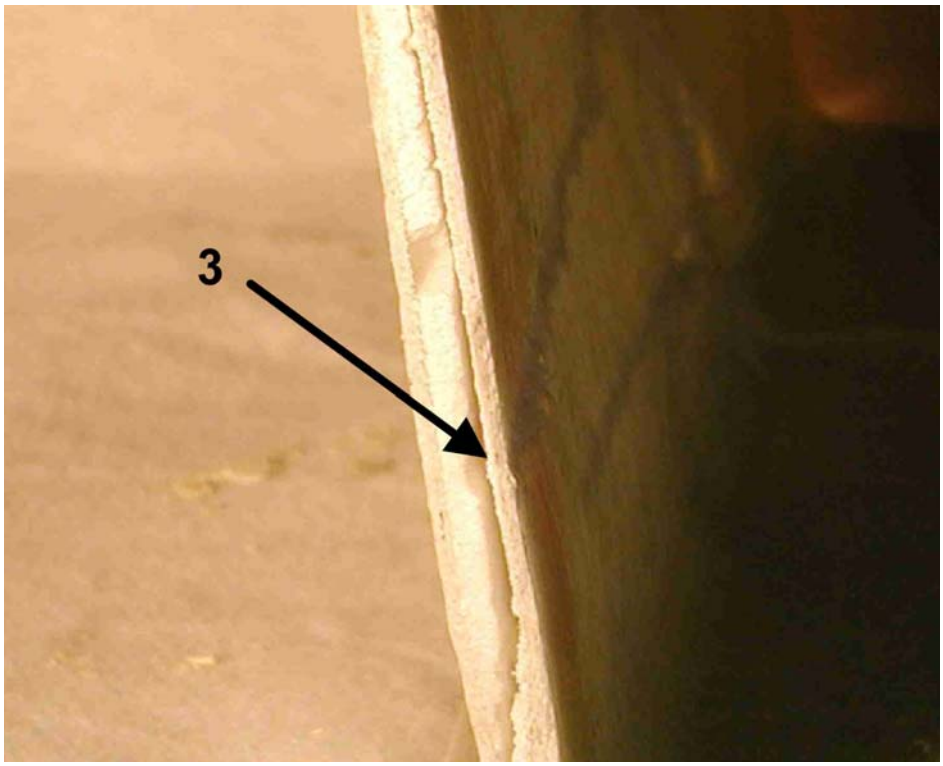

Fig. 3.12: Main spar web sandwich. Damage type 3 (web sandwich panel face/core debonding). *(D - 2-sandwich face-core delam P1290045.jpg)*

4 Finite Element simulation of buckling of a main spar

4.1 Problem definition

The main spar is the primary load carrying structure in the wind turbine blade designed and manufactured by Vestas. A major failure mode is failure of the load carrying fibre composite in compression due to structural buckling. The problem has great complexity and requires geometrical nonlinear analysis. In this project the Finite Element Method (FEM) is used to model the problem. The purpose was to generate general information about the behavior of composite structures subjected to compression.

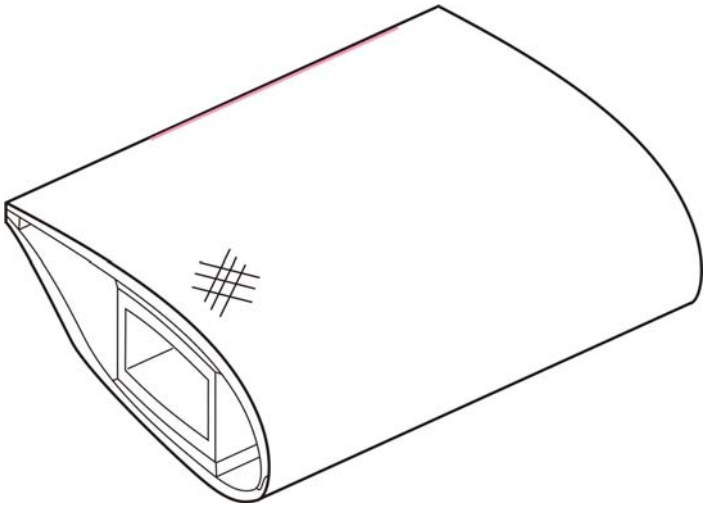

Fig. 4.1. Principle sketch of Vestas blade with main spar

A FEM-model of the main spar is analyzed and results are compared with results from the full-scale test. The geometry is identical to the middle section of a Vestas V52 blade. Shell elements are used. The (anisotropic) stiffness properties of the elements are calculated by the use of laminate theory, modeling an actual construction. The following boundary conditions were used: All displacements were locked at the left end of the model (no degree of freedom) and a single force, pulling in the positive *y*-direction, was applied at the end of the blade, see Fig. 4.2.

The main goal in the work was to get an overview of possible failure mechanism and buckling modes for a wind turbine blade, loaded flap-wise.

Development of damage and failure was not included in the FEM-model. According to a literature survey, interlaminar failure mode (delamination) is expected to be the most important failure mechanism.

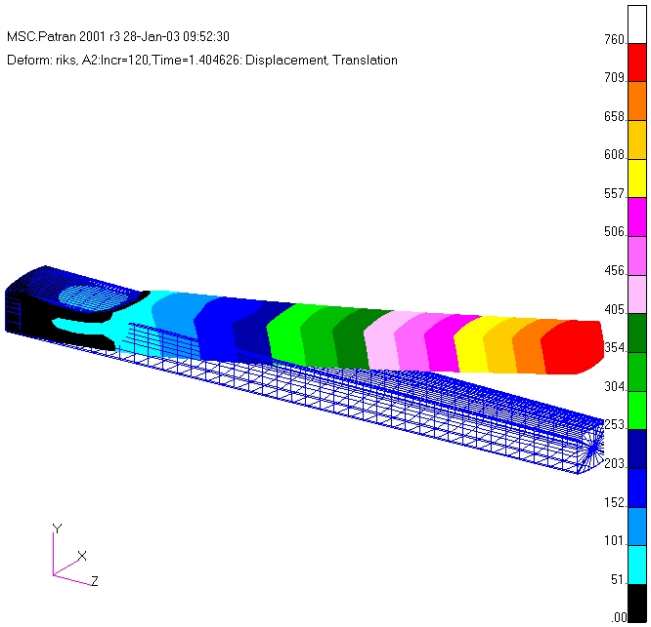

Fig. 4.2. Deformation plot of the model of a main spar. The color indicates the displacements in the y*-direction (in mm).*

4.2 Load-displacement response of the main spar

A deformation plot of the main spar i.e., the relationship between the applied load and the displacement in the load direction (*y*-direction) is shown in Fig. 4.3. The curve exhibits linear behaviour (prebuckling) up to 105 kN where the bifurcation point is reached and a geometrical nonlinear response goes up to 181 kN and the "snap through point" is reached. This "snap through" point is characterized with not having any load-carrying capacity after the limit is reached.

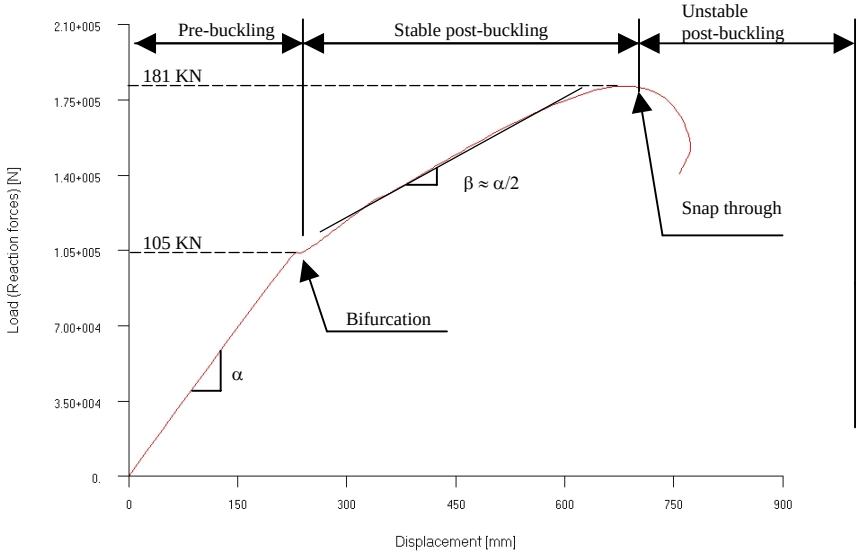

Fig. 4.3. Load-displacement graph of the main spar from FEM-simulation (relationship between applied force and the displacement of the force).

The load-displacement path exhibits stable postbuckling behaviour after the bifurcation point is reached, and the stable postbuckling phase stops at the snap-through load of 181 kN.

4.3 Buckling behaviour (Displacement in the post buckled section)

The deformation plot shows a relatively large local downward deformation of the compression flange, in point A on Fig. 4.4.

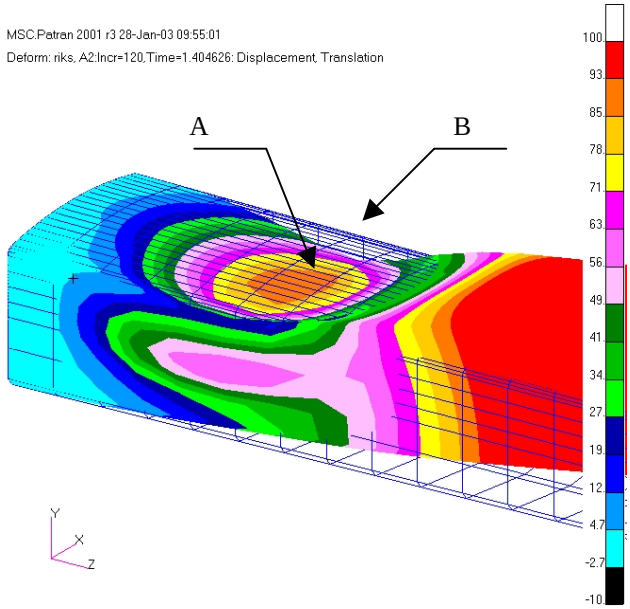

Fig. 4.4. Displacement plot of post buckled section (displacement in the y*-direction). The color range is in mm.*

When the load reaches a certain level, the deflection of the flange, will "snap through". See the three deformations stages in Fig. 4.5.

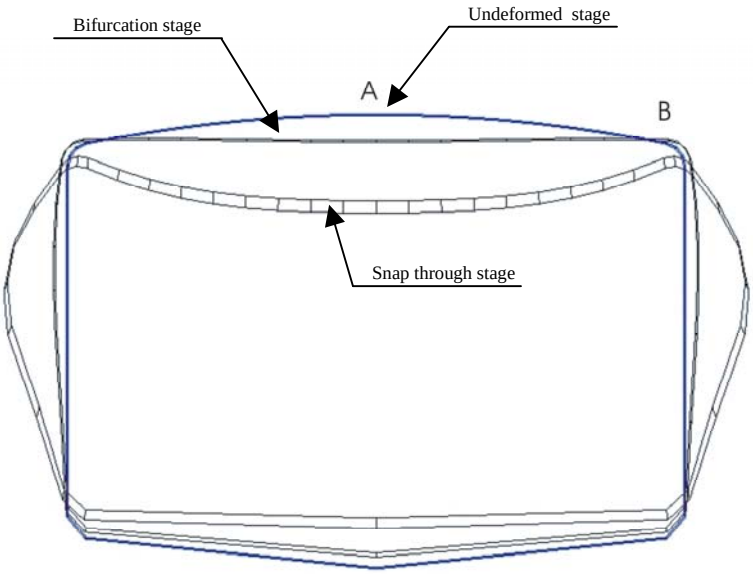

Fig. 4.5. Transverse section of the main spar. Three deformations stages are shown.

Following snap-through, the compression flange will find a new stable equilibrium. See deformation stage 3 in Fig. 4.5, where it can still carry some compression load but on a lower level than before the "snap-through" point was reached. The reduction in load carrying capacity will effect in collapse of the main spar if the surrounded structure does not have the capacity to carry this extra load. In all cases there is an eminent risk that there will be a permanent damage after such a "snap-through" limit has past.

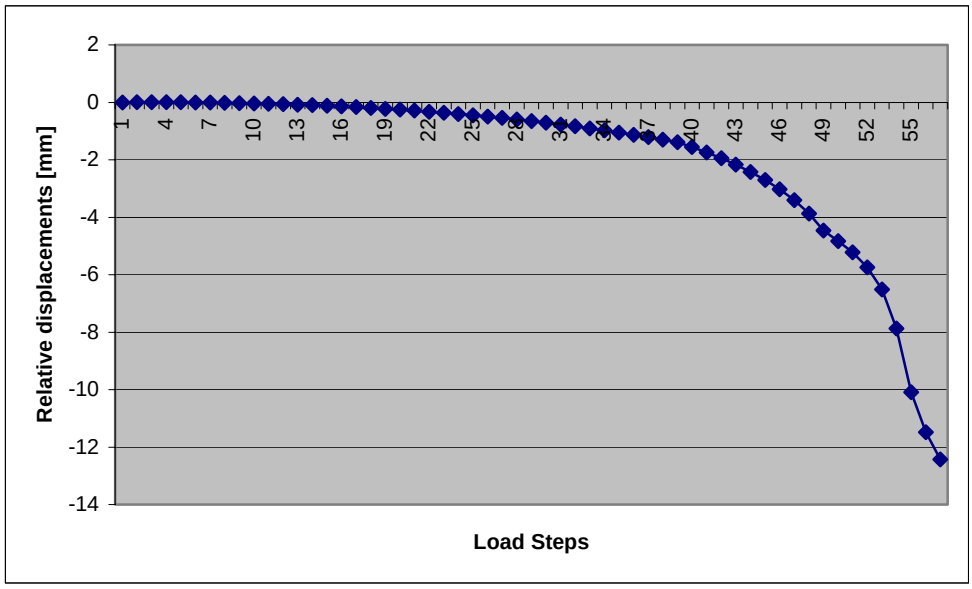

Fig. 4.6. Displacement versus load from the FEM-model. The displacement is in the y-direction where point B is subtracted from point A.

When we compare full-scale measurements Fig. 4.7 and FEM-simulations Fig. 4.6, the "relative deflections" in point A minus point B, show almost the same behaviour, which confirms that we actually have the bifurcation point just before the blade collapses.

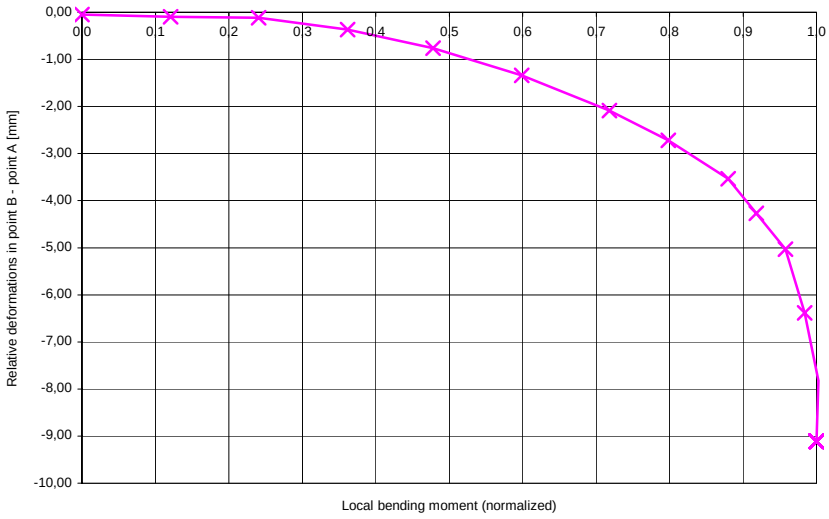

Fig. 4.7: Displacements versus load recorded at the full-scale test (test section 3)

4.4 Summery and conclusions

Compressive stability FEM-simulations of composites are notoriously difficult, and despite the huge amount of research that has been undertaken there are still many problems to solve in the future.

In the FEM-simulation of the main spar, delaminations, imperfections, material degradation are not included. Therefore the result must be handled carefully. The full-scale experiment indicates that significant damage develops prior to failure. A comparison between the full-scale test and FEM-simulation of the buckling behaviour of the compression flange and the load-deflection path has shown the same behaviour to the bifurcation point.

The FEM-simulation of the load-displacement path of the main spar, has shown a stable postbuckling behaviour after the bifurcation point. It can be concluded that strong orthotropic panel without delaminations, imperfection, material degradation and with a small curvature have a stable postbuckling behaviour. In case of no delaminations, the flanges will not be so sensitive to imperfections, but in cases where delaminations develop there will not be a long stable postbuckling behaviour and the load capacity will be sensitive to imperfections.

4.5 Improvements and further work

A lot of improvement can be made in the FEM-simulation, but we believe that it is not realistic the next 3 – 5 years that FEM-models can be developed to give so accurate strength predictions that full-scale testing becomes unnecessary.

But in cases where advanced FEM-models are calibrated with experience from the laboratory and full-scale testing, we believe that it is possible to design the next generation of large blades without any major "surprises" in the final full-scale test. Today we find the FEM-tools, in this complicated area, very useful to improve the understanding of how composites in compression behave, and parameter analysis can show the tendency while changing some geometry or material parameters. Parameter analysis could investigate the buckling behaviour, when geometry, fibre lay-ups, material parameters etc. are changed. Possible improvements of FEM-model of the main spar are:

- Details of the geometry, lay-up, ply drops, etc. must be improved.
- Material degradations must be included, so the stiffness reduction in the lay-up is taken into account.
- Second order shear effects may improve the out of plane shear flexibility.
- Damage evolution (e.g. delamination) should be included.

5 The compressive strength of composite columns

Composites are susceptible to buckling when subject to compression in the direction of the fibres. Work has previously been carried out for columns made of a homogeneous material to study the transition from Euler buckling of long, slender columns to failure by strain localisation or surface bifurcation of short, wide plate segments. A similar study has been carried out for a material with a layered microstructure.

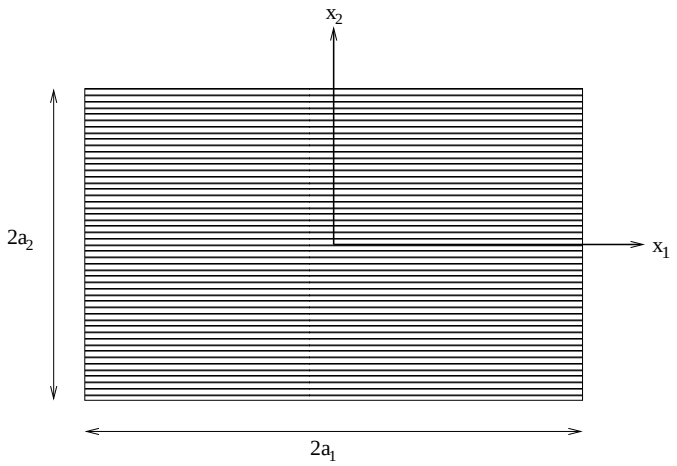

Fig. 5.1 Geometry of the analysed structure.

The constitutive model developed by Christoffersen and Jensen (1996) and Jensen and Christoffersen (1997) has formed the basis of the study. The elliptic, hyperbolic and parabolic regimes for the governing incremental equilibrium equations have been classified. A bifurcation analysis has then been carried out and it is shown that bifurcation stresses precede the critical stress for loss of ellipticity where strain localisation may occur.

In Fig. 5.2 a plot is shown of the bifurcation stress normalised by the elastic shear modulus, *G*, of the composite as a function of the aspect ratio of the column $\gamma_m = \pi a_2/(2a_1)$. The matrix material is described by J_2-flow theory or J_2-deformation theory, and results are shown for different ratios between fibre and matrix stiffness. As the width of the column increases the bifurcation stress converges towards the surface bifurcation stress, which is slightly lower than the critical stress for loss of ellipticity.

In Fig. 5.3 the transition from Euler buckling to surface bifurcation is demonstrated. The Fig. demonstrates the effects of modelling the fibres and matrix as linear or as non-linear with σ_y denoting the yield stress of the materials. Effects of residual stresses on the bifurcation stress have been investigated along with effects of the various material parameters for the matrix, the fibres and the composite material.

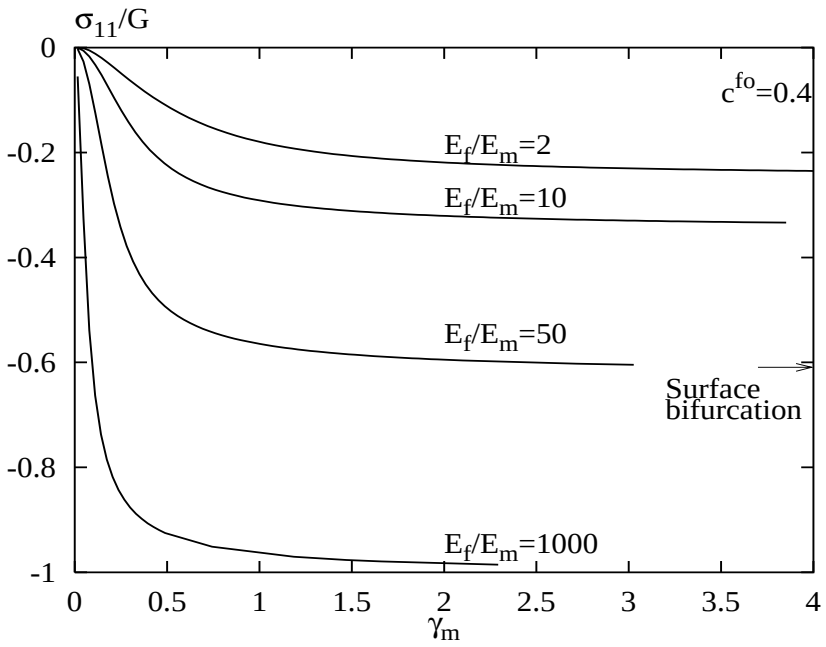

Fig. 5.2 Predicted compressive strength as a function of aspect ratio of the column and various stiffness ratios between fibre and matrix.

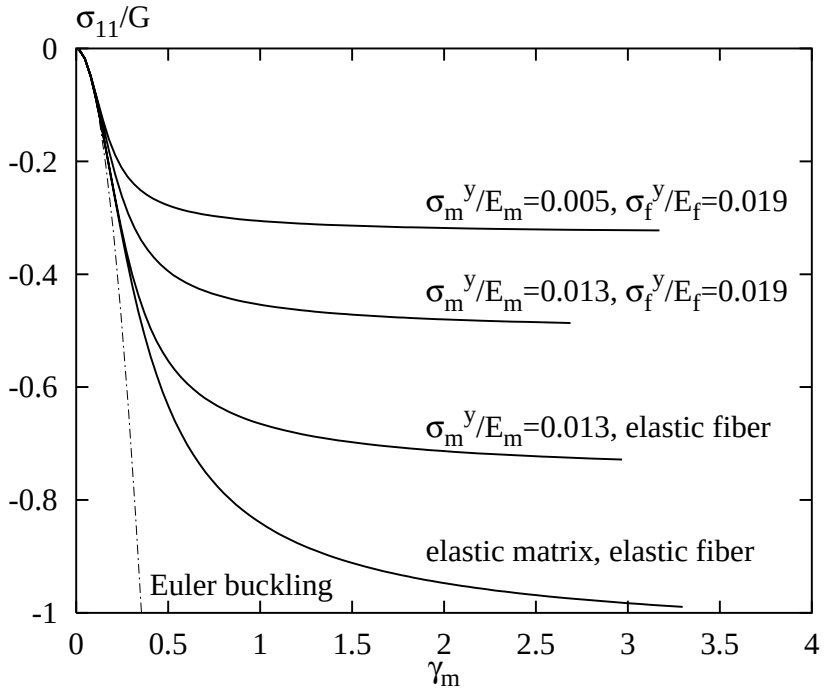

Fig. 5.3 Predicted compressive strength as a function of aspect ratio of the column and yield stress of the matrix and fibre.

6 Fracture mechanics strength characterisation of adhesive joints

6.1 Background and purpose

As discussed above (chapter 3), failure of adhesive joints is a common failure mode in wind turbine blades. Failure of adhesive joints usually occurs as mixed mode cracking, i.e. in a combination of opening ("peel") and tangential (shear") crack opening displacements. Furthermore, mixed mode cracking is often accompanied by fibre bridging in the wake of the crack. The crack bridging can enhance the joint strength significantly and should be taken into account. Therefore, the purposes of the investigations described in this chapter are:

- to develop an experimental method for fracture mechanics characterisation of adhesive joints
- to demonstrate the method by measuring the fracture resistance as a function of loading mode
- to predict the strength of medium-size specimens
- to verify the predictions by measurements of the load-carrying capacity of medium-size specimens

6.2 Development of a mixed mode test specimen

The mixed mode specimen developed in the present study is shown schematically in Fig. 6.1. It enables stable crack growth and the mode mixity can be varied from pure "opening" ("peel") to pure "shear" simply by varying the ratio between the moments, as shown in Fig. 6.2.

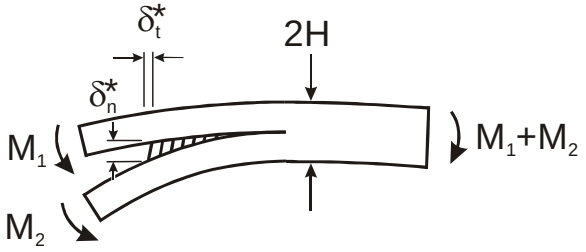

Fig. 6.1 The fracture mechanics test specimen - a double cantilever beam specimen loaded with uneven bending moments. [Mixed_mode_specimens_1e.cdr]

The fracture resistance (energy per unit crack area) can be determined analytically as follows by the use of the J integral (plane stress):

$$J_{ext} = \frac{21\left(M_1^2 + M_2^2\right) - 6M_1M_2}{4B^2H^3E}\ , \qquad (6.1)$$

where M_1 and M_2 are the applied moments at which cracking takes place, E denotes the Young's modulus, B is the specimen width and H is the beam height. The specimen allows stable crack growth, and J can be determined without knowledge of the crack length and remains valid even though a large-scale crack bridging zone (cohesive zone) develops. The most prominent feature of the specimen is, however, that so called cohesive laws, representing the mechanical response of crack bridging by fibres, can be extracted by a J integral approach. The approach, which builds upon an approach used successfully for pure mode I cracking (Sørensen, 2002), is described in detail elsewhere (Sørensen et al., 2003a).

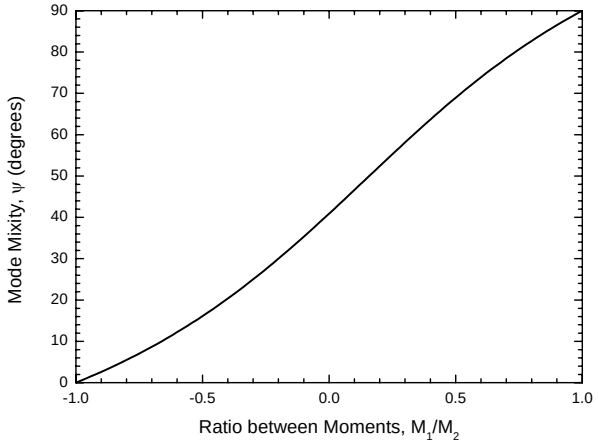

Fig. 6.2 The mode mixity as a function of the ratio between the applied moments. [Moments_mixity_1c.opj]

A special fixture was developed to create the desired loading. The principle is shown in Fig. 6.3. Sandwich specimens, consisting of an adhesive layer joining two glass/polyester laminates were manufactured by LM Glasfiber A/S and tested under various mode mixities.

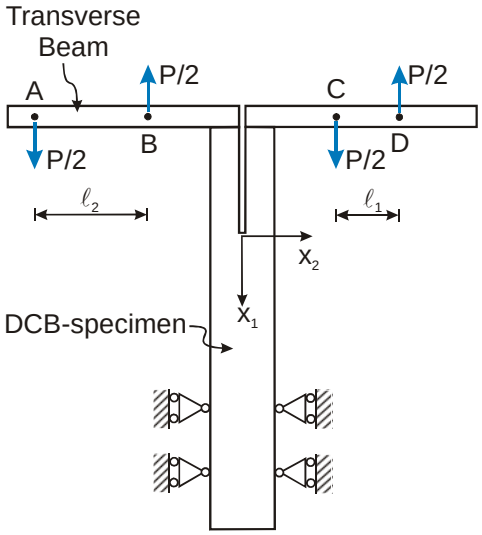

Fig. 6.3 Schematics of the loading method; the mode mixity is controlled entirely by altering the length of one of the transverse beam arms, e.g. ℓ_1. [Mixed_Mode_loading_1b.cdr]

In the first stages of cracking, the crack grew along the adhesive/laminate interface. After about 30 mm growth, another crack formed in the laminate at the interface between the first surface lamina and the one below. At both cracking planes, fibre bridging was observed. The fibre bridging resulted in rising crack growth resistance with increasing crack length (R-curve behaviour) until a steady state value J_{ss} was reached. The measure steady-state fracture resistance is shown in Fig. 6.4 as a function of the ratio between the end-sliding and end-opening of the cohesive zone (see Fig. 6.1), δ_n^* and δ_t^*, expressed through the phase angle $\varphi = \tan^{-1}(\delta_t^* / \delta_n^*)$. Observe that J_{ss} is almost constant - independent of the loading ratio - until φ approaches unity ("mode II").

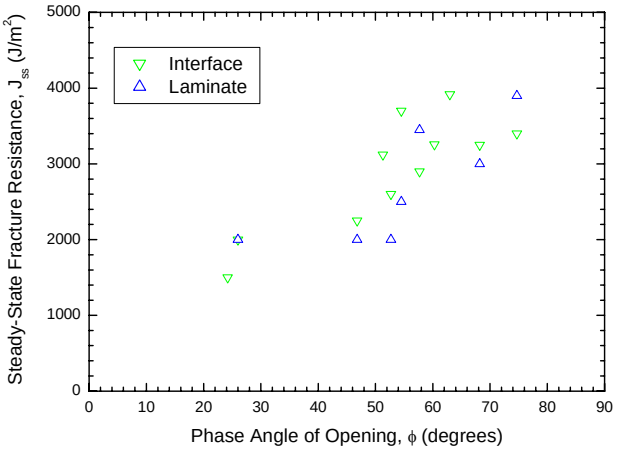

Fig. 6.4 Measured steady-state fracture resistance as a function of $\varphi = \tan^{-1}(\delta_t^* / \delta_n^*)$. *Tending towards "mode II"* $\varphi > 50°$, *the steady-state fracture resistance increases significantly. [File =Mixed_mode_results_overview_1c.opj]*

6.3 Medium size specimens: strength prediction and strength measurements

Medium-size specimens were manufacture by LM Glasfiber A/S and tested in four-point bending to determine their load carrying capabilities. The geometry and loading of the specimens are shown in Fig. 6.5. The specimens consist of two plates (of thickness *h* and *H*, respectively). The length of the longest part was 2000 mm and the width, *B*, was 60 mm nominally, and the thickness, *H*, was nominally 60 mm.

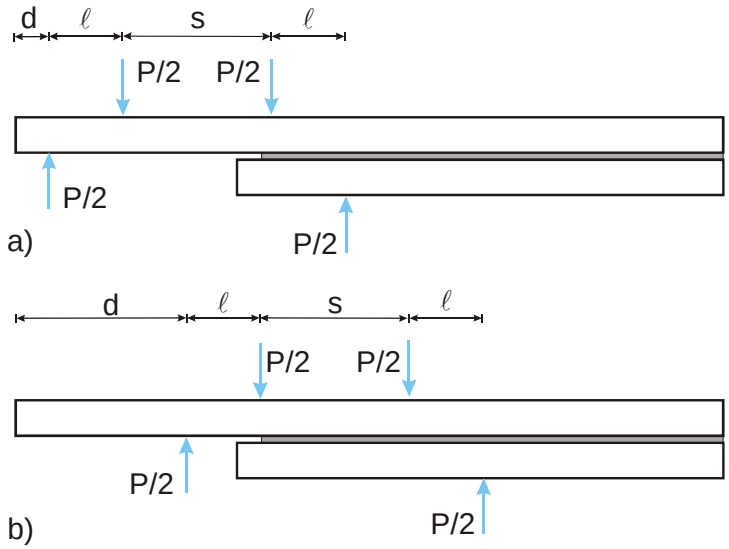

Fig. 6.5. The loading principles for crack initiation (a) and crack propagation (b). (UCSB_emne_1a.cdr)

The critical moment at steady-state cracking of the medium size specimens, M_c, is predicted to be (Sørensen et al., 2003b)

$$\frac{M_c}{B\sqrt{J_{ss}H^3E}} = \frac{1}{\sqrt{6}\sqrt{1-\frac{1}{\left(1+h/H\right)^3}}}, \qquad (6.2)$$

where M_c is the critical at steady-state crack growth, E denotes the Young's modulus, B is the specimen width and h and H is the height of the two beams. A prediction of a normalised M_c is shown as a solid curve in Fig. 6.6. The predictions are based on the measurements at the smaller laboratory specimens described in Section 6.2 (Sørensen et al., 2003a). Note, that the model predicts that a reduction in the thickness of the thinner beam, h, gives a higher joint strength. Comparing the measured and predicated strength values, it is found that they are in good agreement. The predicted trend that a decreasing h/H should lead to an increase in M_c is confirmed by the measurements.

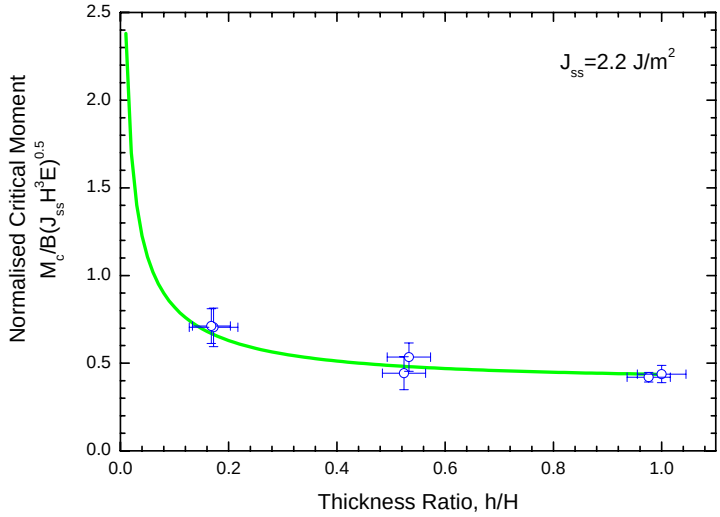

Fig. 6.6. Predicted (solid line) and measured maximum (steady-state) values (points) of applied moment at crack growth as a function of thickness ratio, h/H. *(UCSB_thickness_1e.opj)*

6.4 Summary and conclusions

A new mixed mode test specimen was successfully developed and applied to fracture mechanics characterisation of adhesive joints. The fracture resistance increased with crack length due to fibre bridging; the steady-state value depended on the ratio between the applied moments, M_1/M_2.

The steady-state failure moment, M_c, of medium size specimens was successfully predicted from fracture date determined from much smaller laboratory specimens. However, the incipient crack growth behaviour of the medium-size specimens cannot be predicted without a numerical (e.g. FEM) model.

The developed test method has potential for also characterisation the fracture resistance and cohesive laws of splitting and delamination in fibre composites under static loading. Future studies should also address fatigue crack growth to clarify whether or not fibre bridging is beneficial for crack growth under cyclic loading.

7 Modelling of crack growth in adhesive joints having air bubbles

7.1 Introduction

The strength of adhesive bonds may be significantly reduced by imperfections such as airbubbles entrapped prior to curing. In the present work (Feraren and Jensen, 2003), a general numerical tool for studying crack growth near flaws of arbitrary shape has been developed. In a previous work (Jensen, 2002) a numerical method for studying crack growth in an adhesive bond was developed. This method was based on a fracture mechanical formulation, which imposes restrictions on the size of the plastic zone in the adherends, the radius of curvature of the crack front etc. These restrictions may not always be satisfied in real, bonded systems and for this reason the present work has focussed on developing a less restrictive numerical tool. The method is based on a cohesive zone model rather than a classical fracture mechanical approach. In the limit where the size of the cohesive zone tends to zero relative to other relevant geometrical measures, results based on the cohesive zone model should converge towards results based on the fracture mechanical model, and a comparison with results in Jensen (2001), Jensen (2002) and Jensen (2003) shows perfect agreement.

7.2 Model results

Results for quasi-static crack propagation in the system illustrated in the Fig. 7.1 are now shown. Two plates are bonded in the overlapping region, but the bond contains a periodic arrangement of elliptic (including circular) voids.

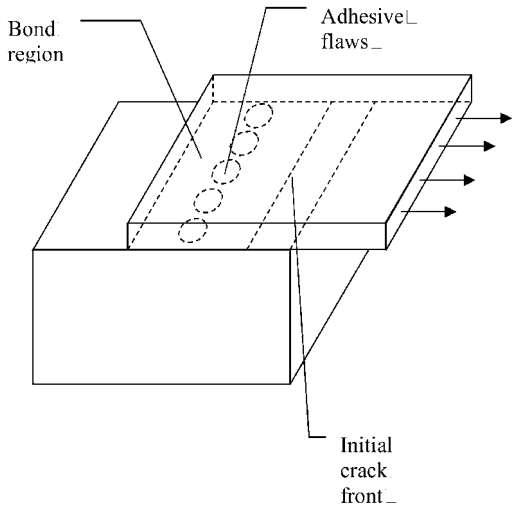

Fig. 7.1 Geometry of the problem: crack growth in an adhesive layer approaching air bubbles. (HMJ_geo1.ps)

Results for the shape of the crack front and the variation of the stress necessary to make the crack propagate are obtained. Fig. 7.2 shows the variation of the stress required for crack propagation for three different cohesive laws as a function of the relative area change of the bonded region. The stress must be increased to initiate crack propagation. The stress then reaches a constant value where the crack propagates as a plane strain edge crack under steady-state conditions. However, as the crack approaches the imperfections the strength of the bond is reduced until the crack has propagated all the way through the flaws.

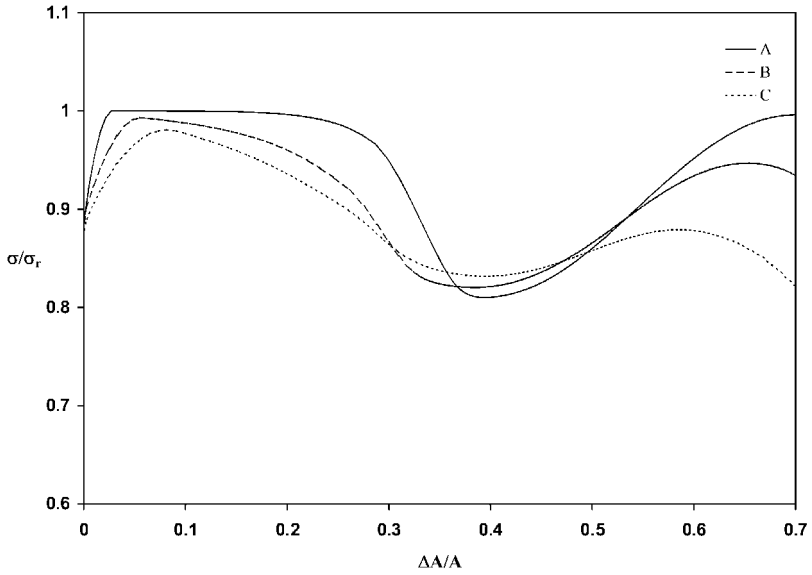

Fig. 7.2 Required applied stress required to propagate the crack front stably past air bubbles as a function of the cracked area. (HMJ_cirkela-b-c2.ps)

8 Summary of major findings

The main results of the project are:

- The development of a new full-scale testing approach allowing three independent failures to be generated in a single wind turbine blade.
- The demonstration of the capability of Acoustic Emission (AE) as a powerful damage detection tool.
- An overview was created of the damage types that can develop in a turbine blade at the structural level. The damage types comprises cracking along adhesive layers, sandwich face/core debonding, composite cracking along fibres (splitting) as well as compression failure of the laminate, delamination of plies of a laminate, and cracks in the gel coat.
- FEM modelling was found to be a very useful tool, giving insight into the behaviour of wind turbine blades during structural buckling.
- The compression strength of composite columns was predicted as a function of column aspect ratio and stiffness ratio of the orthotopic plate.
- Modelling results showed how porosity decreases the strength of adhesive joints.
- A new fracture mechanics design criterion was developed for adhesive joints. Results from small laboratory specimens were used to predict the load carrying capability of much larger specimens, showing that the design approach can predict scale effects correctly.

The project has thus established a solid foundation for the development of new design methods for wind turbine blades made of fibre composites. A number of the damage modes that were found in blades tested to failure were not investigated in details in the present study. Robust design criterion must also be developed for those damage modes, so that the blade designer in the future has all the necessary tool required to design his blade against any relevant failure mode and thus can optimise his construction details for optimal strength.

9 List of publications

This list contains references to papers that were published or made during the project.

Debel, C. P., 2004, "Identification of Damage Types in Wind Turbine Blades Tested to Failure", Risø-R-1391(EN).

Gamstedt, E.K., Sørensen, B.F., 2002. "Interaction of damage development and dissipation in tensile fatigue loading of composite laminates". In: Durability analysis of composite systems 2001. DURACOSYS 2001, Miyano, Y.; Cardon, A.H.; Reifsnider, K.L.; Fukuda, H.; Ogihara, S. (eds.), (A.A. Balkema Publishers, Lisse, 2002) p. 213-220.

Hansen, P. F., and Jensen, H. M., "2-D Cohesive Zone Modelling of Interface Fracture near Flaws in Adhesive Bonds", (2003). Submitted.

Jacobsen, T.K., Andersen, L.F., Sørensen, B.F., Jensen, H.M., Hansen, P.F., "Brudmekanisk karakterisering og design af limsamlinger". In: Karakterisering af materialer - fra atom til makro. Dansk Metallurgisk Selskabs vintermøde, Kolding (DK), 2-4 Jan 2002. Brøndsted, P.; Somers, M.A.J. (eds.), (DMS, Lyngby, 2002) p. 61-73.

Jensen, F. M., et al., "Compression Strength of a Fibre Composite Main Spar in a Wind Turbine Blade", Risø-R-1393(EN).

Jensen, H. M., "Crack Initiation and Growth in Brittle Bonds". *Engineering Fracture Mechanics* **70**, 1611-1621, 2003.

Jensen, H. M., "Free Edge and Interaction Effects on the Strength of Finite-Sized Interface Bonds", Advances in Fracture Research, (Eds. K. Ravi-Chandar, B.L. Karihaloo, T. Kishi, R.O. Ritchie, A.T. Yokobori Jr., T. Yokobori), 2001, 6p.

Jensen, H. M., "Residual Stress Effects on the Compressive Strength of Uni-directional Fibre Composites". *Acta Materialia* **50**, 2895-2904, 2002.

Jensen, H. M., "Three Dimensional Numerical Investigation of Brittle Bond Fracture". *International Journal of Fracture* **114**, 153-165, 2002.

Jensen, H. M., and Sheinman, I. "Numerical Analysis of Buckling-Driven Delamination". *International Journal of Solids and Structures* **39**, 3373-3386, 2002.

Jensen, H. M.,"Compressive Failure of Fibre Reinforced Materials". DCAMM Symposium on Challenges in Applied Mechanics, (Eds. N. Olhoff and P. Pedersen), in press.

Jørgensen, E., et al., "Full scale testing of wind turbine blade to failure - flapwise loading", Risø-R-1392(EN).

Lilholt, H., Madsen, B., Toftegaard, H., Cendre, E., Megnis, M., Mikkelsen, L.P., Sørensen, B.F. (editors), 2002, Sustainable natural and polymeric composites - science and technology. Proceedings. 23. Risø international symposium on materials science, Risø (DK), 2-5 Sep 2002. (Risø National Laboratory, Roskilde, 2002) 371 p.

Moon, M.-W., Jensen, H. M., Hutchinson, J. W., Oh, K. H., and Evans, A.G. "The Characterization of Telephone Cord Buckling of Compressed Thin Films on Substrates". *Journal of the Mechanics and Physics of Solids* **50**, 2355-2377, 2002.

Pane, I., and Jensen, H. M., "Plane Strain Bifurcation and its Relation to Kink Band Formation in Layered Materials", (2003). Submitted.

Panthleon, K., Somers, M.A.J., Horsewell, A., Jensen, H. M., and Pane, I. "Measurement and Modelling of Stress Distributions and Failure in Finite Structures", (2003) Under udarbejdelse.

Sørensen, B. F., Jørgensen, K., Jacobsen, T. K., and Østergaard, R. C., 2003, "A general mixed mode fracture mechanics test specimen for characterising adhesive joints", Risø-R-1394(EN), Risø National Laboratory, Roskilde, Denmark.

Sørensen, B. F., "Cohesive law and notch sensitivity of adhesive joints", *Acta Materialia*, **50**, 1053-61, 2002.

Sørensen, B. F., and Jacobsen, T. K., 2003, "Determination of cohesive laws by the J integral approach", *Engineering Fracture Mechanics* **70**, 1841-58.

Sørensen, B. F., and Jacobsen, T. K., 2003, "Fracture mechanics characterisation of medium-size adhesive joint specimens", Risø-R-1411(EN), Risø National Laboratory, Roskilde, Denmark.

Sørensen, B. F., Jørgensen, E., Debel, C. P., Jensen, F. M. and Jensen, H. M., 2003,"Improved design of large wind turbine blade of fibre composites based on studies of scale effects (Phase 1) - Summary Report", Risø-R-1390(EN).

Sørensen, B.F., and Jacobsen, T.K., 2002, "Crack bridging in composites: Connecting mechanisms, micromechanics and macroscopic models". In: Proceedings. Vol. 2. International conference on new challenges in mesomechanics (Mesomechanics 2002), Aalborg (DK), 26-30 Aug 2002. Pyrz, R.; Schjødt-Thomsen, J.; Rauhe, J.C.; Thomsen, T.; Jensen, L.R. (eds.), (Aalborg University, Aalborg, 2002) p. 599-604.

Østergaard, R. C., and Sørensen, B. F., "Interface crack in isotropic sandwich structures", *Int. J. Fracture*. To be submitted.

10 Other references

Christensen, C. J., Ronold, K. O., and Thøgersen, M.L., 2000, "Calibration of partial safety factors for design of wind-turbines rotors blades against fatigue failure in flapwise bending", Risø-R-1204(DA).

Christoffersen, J., and Jensen, H. M., 1996, "Kink Band Analysis Accounting for the Microstructure of Fiber Reinforced Materials", *Mechanics of Materials* **24**, pp. 305-315.

Jensen, H. M., 1999, "Analysis of Compressive Failure of Layered Materials by Kink Band Broadening", *International Journal of Solids and Structures* **36**, pp. 3427-3441.

Jensen, H. M., 1999, "Models of Failure in Compression of Layered Materials", *Mechanics of Materials* **31**, pp. 553-564.

Jensen, H. M., and Christoffersen, J., 1997, "Kink Band Formation in Fiber Reinforced Materials", *Journal of the Mechanics and Physics of Solids* **45**, pp. 1121-1136.

Mission

To promote an innovative and environmentally sustainable technological development within the areas of energy, industrial technology and bioproduction through research, innovation and advisory services.

Vision

Risø's research **shall extend the boundaries** for the understanding of nature's processes and interactions right down to the molecular nanoscale.

The results obtained shall **set new trends** for the development of sustainable technologies within the fields of energy, industrial technology and biotechnology.

The efforts made **shall benefit** Danish society and lead to the development of new multi-billion industries.